PERGAMON

International Journal of Heat and Mass Transfer 44 (2001) 1411–1423

International Journal of HEAT and MASS TRANSFER

www.elsevier.com/locate/ijhmt

Non-spherical bubble collapse mechanics in binary solutions

J. Cao *, R.N. Christensen

Department of Mechanical Engineering, The Ohio State University, 206 W. 18th Avenue, Columbus, OH 43210, USA

Received 29 October 1999; received in revised form 17 April 2000

Abstract

Mechanics of bubble collapse in binary mixtures with heat and mass transfer has been investigated in this paper. The flow field surrounding a collapsing bubble undergoing buoyancy-driven motion was solved using adaptive finite-difference method. A curvilinear coordinate system is employed to keep track of the changing bubble shape. The moving boundary feature is considered as an integral part of the governing equations. The bubble collapse rate, velocity, temperature and species concentration field, and simulation of the bubble collapsing process have been reported.

1. Introduction

Bubbles, as fluid particles, are of importance in a host of physical and chemical processes that involve gas–liquid interaction. Bubble collapse is one of the primary phenomena occurring in bubble column reactors and bubble absorbers in the absorption refrigeration systems. The fluid mechanics of bubble collapse, upon which the heat and mass transfer are strongly dependent, is particularly complex and its knowledge is limited. So far, there are only few reported results on spherical bubble collapse based on potential flow assumptions [1,2].

An important analytical solution for flow around fluid spheres was given by Hadamard [3] and Rybczynski [4]. The solution is derived for slow viscous flow past fluid spheres when the viscous effect is so pronounced that the bulk convection can be neglected, namely creeping flow. As the *Re* increases, the creeping flow condition no longer exists. Levich [5] adopted boundary layer theory and predicted the velocity profile near the bubble surface. His work was later proved valid up to *Re* of 200 by Hamielec et al. [6] using finite difference method. Brabston [7] also studied the steady viscous flow past a fixed size spherical gas bubble for *Re* in the range of $0.1 < Re < 200$. He used the method of series truncation to reduce the problem to a nonlinear boundary value problem, then solved it by the finite difference method. Bubble shapes may be altered when the bubble rises through the ambient liquid. The deformation of bubbles is subject to the external flow field until normal and shear stresses reach balance at the interface. Generally, a bubble in an unbounded Newtonian fluid may take one of the following shapes during its life span: spherical, ellipsoidal, ellipsoidal-cap and spherical-cap. Clift et al. [8] provided a shape regime map for bubbles and drops. Bubbles are ellipsoidal at relatively high *Re* and intermediate *Eo* ($= \Delta\rho g d_e^2/\sigma$), spherical- or ellipsoidal-cap at high *Re* and *Eo*. Large bubbles and drops tend to have flat bases and lack the semblance of fore-and-aft symmetry. These fluid particles usually have "spherical-cap" or "ellipsoidal-cap" shape.

Ryskin et al. [9,10] developed a numerical scheme to investigate the wake structures behind fixed size ellipsoidal and spherical-cap bubbles under steady-state condition. It was shown that the bubble shape and the velocity and pressure fields in the fluid are intimately interconnected. Later, Takagi et al. [11] extended Ryskin's results to unsteady-state condition.

Florschuetz [12] made use of Plesset–Zwick [13] temperature integral and identified that bubble collapse could be controlled by heat transfer or liquid inertia in a single component system. For bubble collapse at moderate temperature difference between the vapor and the

* Corresponding author. Tel.: +1-614-292-0812; fax: +1-614-688-9046.

E-mail address: cao.30@osu.edu (J. Cao).

0017-9310/01/$ - see front matter
PII: S0017-9310(00)00147-2

Nomenclature

a	semimajor axis
b	semiminor axis
d	bubble diameter (m)
D_0	initial bubble diameter (m)
D_{ij}	mass diffusivity ($m^2\ s^{-1}$)
Eo	Eotvos number ($=\Delta\rho g d_e^2/\sigma$)
h	enthalpy ($J\ kg^{-1}$) or bubble surface profile
Δh_{lv}	heat released per unit mass of vapor absorbed ($J\ kg^{-1}$)
J	Jacobian term
Ja	Jakob number ($=\rho_l C_{pl}\Delta T/\rho_v(h_v-h_l)$)
k	conductivity ($W\ m^{-1}\ K^{-1}$)
$\dot{m}$	mass reduction rate ($=dm/dt$) ($kg\ s^{-1}$)
Mo	Morton number ($=\mu^4 g\Delta\rho/\rho^2\sigma^3$)
n	normal direction
p	pressure (Pa)
Pr	Prandtl number ($=\nu/\alpha$)
r	axisymmetric coordinate
R	bubble radius (m)
$\dot{R}$	bubble collapsing rate ($=dR/dt$) ($m\ s^{-1}$)
Re	Reynolds number ($=\rho U t D_0/\mu$)
Sc	Schmidt number ($=\nu/D_{ij}$)
t	time (s) or tangential direction
T	temperature (K)
$\mathbf{T}$	stress tensor
u	velocity component in r direction ($m\ s^{-1}$)
U_t	bubble terminal velocity ($m\ s^{-1}$)
U^*	contravariant velocity component
v	velocity component in z-direction ($m\ s^{-1}$)
V^*	contravariant velocity component
$v_{l,n}$	normal velocity of liquid at the interface ($m\ s^{-1}$)
We	Weber number ($=\rho U_t^2 d/\sigma$)
z	axisymmetric coordinate

Greek symbols

α	thermal diffusivity ($m^2\ s^{-1}$)
γ	curvilinear coordinate component
η	curvilinear coordinate component
φ	normalized mass concentration ($=(\omega-\omega_\infty)/\omega_\infty$)
θ	dimensionless temperature
μ	dynamic viscosity ($kg\ m^{-1}\ s^{-1}$)
ν	kinematic viscosity ($m^2\ s^{-1}$)
ρ	total density of liquid, i.e., ρ_l ($kg\ m^{-3}$)
σ	surface tension ($N\ m^{-1}$)
τ	stress (Pa)
ω_i	mass concentration of ammonia ($=\rho_i/\rho$)
ω_j	mass concentration of water
ξ	curvilinear coordinate component
ψ	dimensionless stream function
ζ	dimensionless vorticity

Subscripts

0	initial value
e	equivalent
i	ammonia
j	water
l	liquid
s	interface
v	vapor
∞	ambient

subcooled liquid, the heat transfer dominates the volumetric decrease of the bubble. Using holographic interferometry and high-speed cinematography, Chen et al. [14] measured the heat transfer at the interface of vapor bubbles condensing in a subcooled liquid of the same substance. Their experiment suggests that bubble collapse can be considered heat transfer controlled if Jakob number is below 60.

Vapor bubbles absorbed into subcooled multi-component solutions are common occurrences in absorbers and other gas–liquid contacting equipment. Combined heat and mass transfer adds some complexity to the bubble absorption problem. But the major difficulty still lies in obtaining accurate description of fluid motion around a non-spherical collapsing bubble. The impact of the flow field on the collapse rate has been recognized but little is known. This paper examined the importance of three factors in bubble collapse dynamics: non-spherical bubble shape, fluid dynamics around a collapsing bubble and absorption in binary solutions.

2. Problem formulation

We are concerned with the specific problem of the buoyancy-driven motion of a single bubble in an unbounded quiescent binary fluid accompanied by the bubble collapse due to the subcooling of the ambient liquid. The fluid is assumed to be Newtonian. The bubble undergoes translatory movement without oscillation at its terminal velocity. The bubble volume decreases as heat and mass transfer occurs through the interface. Since mass diffusion causes heat-release during an exothermic process, heat transfer near the bubble surface has phenomenal impact on the mass transfer. Inside the bubble, the temperature and concentration distributions are presumed to be uniform. This is supported by the fact that the internal circulation facilitates creating uniform fields. Outside the bubble, the liquid is assumed to be incompressible and have constant thermodynamic and transport properties except for temperature and concentration. At the bubble interface, thermal equilibrium prevails and free surface is assumed.

Since the bubble shape is normally axisymmetric, the flow around the bubble is also assumed axisymmetric.

The collapsing process starts immediately after a bubble is introduced into a subcooled liquid. From an observer's point of view, the bubble is rising through the quiescent liquid. But it can also be viewed as the liquid flowing past a stationary bubble. The formulation of the problem is facilitated by choosing the centroid of the bubble as the origin of the coordinate system. In line with the above assumptions, the governing equations can be expressed as

$$\frac{\partial(r\mathbf{Q})}{\partial t}+\frac{\partial(r\mathbf{E})}{\partial r}+\frac{\partial(r\mathbf{F})}{\partial z}=\frac{\partial(r\mathbf{E}_{\mathrm{v}})}{\partial r}+\frac{\partial(r\mathbf{F}_{\mathrm{v}})}{\partial z}+r\mathbf{H}, \tag{1}$$

where

$$\mathbf{Q}=\begin{pmatrix}\rho\\ \rho u\\ \rho v\\ \rho e\\ \rho_i\end{pmatrix},\quad \mathbf{E}=\begin{pmatrix}\rho u\\ \rho uu\\ \rho uv\\ \rho ue\\ \rho_i u\end{pmatrix},\quad \mathbf{F}=\begin{pmatrix}\rho v\\ \rho uv\\ \rho vv\\ \rho ve\\ \rho_i v\end{pmatrix}, \tag{2}$$

$$\mathbf{E}_{\mathrm{v}}=\begin{pmatrix}0\\ \tau_{rr}\\ \tau_{zr}\\ -q_r\\ -j_{ir}\end{pmatrix},\quad \mathbf{F}_{\mathrm{v}}=\begin{pmatrix}0\\ \tau_{rz}\\ \tau_{zz}\\ -q_z\\ -j_{iz}\end{pmatrix},\quad \mathbf{H}=\begin{pmatrix}0\\ -\tau_{\theta\theta}/r\\ -\rho g\\ 0\\ 0\end{pmatrix}, \tag{3}$$

$$\begin{aligned}&\tau_{rr}=-p+2\mu\frac{\partial u}{\partial r},\quad q_r=-k\frac{\partial T}{\partial r},\\ &\tau_{zz}=-p+2\mu\frac{\partial v}{\partial z},\quad q_z=-k\frac{\partial T}{\partial z},\\ &\tau_{rz}=\tau_{zr}=\mu\left(\frac{\partial v}{\partial r}+\frac{\partial u}{\partial z}\right),\quad j_{ir}=-D_{ij}\frac{\partial\rho_i}{\partial r},\\ &\tau_{\theta\theta}=-p+2\mu\frac{u}{r},\quad j_{iz}=-D_{ji}\frac{\partial\rho_i}{\partial z}.\end{aligned} \tag{4}$$

The axisymmetric coordinates being used is shown in Fig. 1 wherein z-axis is the symmetric axis about which the oblate object is formed by revolution. The subscripts i and j refer to species i and j, respectively. $D_{ij}=D_{ji}$ denotes mass diffusivity.

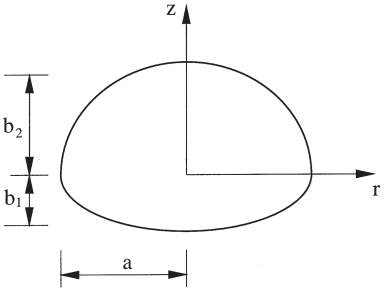

Fig. 1. Axisymmetric coordinate system.

The governing equations can be expanded and transformed into non-dimensional form by introducing the following non-dimensional variables:

$$r'=\frac{r}{D_0},\quad z'=\frac{z}{D_0},\quad t'=\frac{U_{\mathrm{t}}t}{D_0},$$

$$u'=\frac{u}{Ut},\quad v'=\frac{v}{U_{\mathrm{t}}},\quad p'=\frac{p}{\rho U_{\mathrm{t}}^2},\quad \theta=\frac{T-T_\infty}{T_\infty},\quad \varphi_i=\frac{\omega_i-\omega_{i\infty}}{\omega_{i\infty}},$$

$$Re=\frac{\rho UtD_0}{\mu},\quad Pr=\frac{\nu}{\alpha},\quad Sc=\frac{\nu}{D_{ij}},\quad Fr=\frac{U_{\mathrm{t}}^2}{gD_0}. \tag{5}$$

D_0 is the initial diameter of the bubble and U_{t} is the bubble terminal velocity, the magnitude of U_{t} ranges from 0.20 to 0.30 m/s. Bubble terminal velocity normally is not constant and depends on many factors including bubble shape and size, etc. But experimental evidence shows that the bubble moves with a nearly constant velocity over a major portion of its life span. For the bubble diameter from 1 to 20 mm, which is the range we are most interested in, the bubble terminal velocity is nearly unchanged [8]. Chen and Mayinger [14] used high-speed cinematography technique studying heat transfer around a condensing bubble. Their experiment demonstrated that the bubble reaches a constant equilibrium velocity shortly after detaching from the nozzle. In practice, many correlations have been developed to predict terminal velocity among which Grace's correlation is used in this paper [8].

After dropping the prime for simplicity, we arrive at the dimensionless governing equations:

(a) *continuity equation*

$$\frac{\partial(ru)}{\partial r}+\frac{\partial(rv)}{\partial z}=0, \tag{6}$$

(b) *r-momentum equation*

$$\begin{aligned}&\frac{\partial u}{\partial t}+u\frac{\partial u}{\partial r}+v\frac{\partial u}{\partial z}=-\frac{\partial p}{\partial r}+\frac{1}{Re}\left(\nabla^2u-\frac{u}{r}\right)\\ &\quad=-\frac{\partial p}{\partial r}+\frac{1}{Re}\left\{\frac{\partial}{\partial r}\left[\frac{1}{r}\frac{\partial}{\partial r}(ru)\right]+\frac{\partial^2u}{\partial z^2}\right\},\end{aligned} \tag{7}$$

(c) *z-momentum equation*

$$\begin{aligned}&\frac{\partial v}{\partial t}+u\frac{\partial v}{\partial r}+v\frac{\partial v}{\partial z}=-\frac{\partial p}{\partial z}+\frac{1}{Re}\nabla^2v-\frac{1}{Fr}\\ &\quad=-\frac{\partial p}{\partial z}+\frac{1}{Re}\left\{\frac{1}{r}\frac{\partial}{\partial r}\left(r\frac{\partial v}{\partial r}\right)+\frac{\partial^2v}{\partial z^2}\right\}-\frac{1}{Fr},\end{aligned} \tag{8}$$

(d) *energy equation*

$$\begin{aligned}&\frac{\partial\theta}{\partial t}+u\frac{\partial\theta}{\partial r}+v\frac{\partial\theta}{\partial z}=\frac{1}{RePr}\nabla^2\theta\\ &\quad=\frac{1}{RePr}\left\{\frac{1}{r}\frac{\partial}{\partial r}\left(r\frac{\partial\theta}{\partial r}\right)+\frac{\partial^2\theta}{\partial z^2}\right\},\end{aligned} \tag{9}$$

(e) *species continuity equation*

$$\frac{\partial \varphi_i}{\partial t}+u\frac{\partial \varphi_i}{\partial r}+v\frac{\partial \varphi_i}{\partial z}=\frac{1}{ReSc}\nabla^2\varphi_i = \frac{1}{ReSc}\left\{\frac{1}{r}\frac{\partial}{\partial r}\left(r\frac{\partial \varphi_i}{\partial r}\right)+\frac{\partial^2\varphi_i}{\partial z^2}\right\}, \tag{10}$$

where

$$\nabla^2=\frac{1}{r}\frac{\partial}{\partial r}\left(r\frac{\partial}{\partial r}\right)+\frac{\partial^2}{\partial z^2}=\frac{\partial^2}{\partial r^2}+\frac{1}{r}\frac{\partial}{\partial r}+\frac{\partial^2}{\partial z^2}. \tag{11}$$

The axisymmetric assumption allows us to transform the momentum equations given above into the stream function-vorticity type

$$\frac{\partial \zeta}{\partial t}+\frac{\partial(u\zeta)}{\partial r}+\frac{\partial(v\zeta)}{\partial z}=\frac{1}{Re}\left\{\frac{\partial}{\partial r}\left[\frac{1}{r}\frac{\partial}{\partial r}(r\zeta)\right]+\frac{\partial^2\zeta}{\partial z^2}\right\}, \tag{12}$$

$$\frac{\partial^2\psi}{\partial r^2}-\frac{1}{r}\frac{\partial \psi}{\partial r}+\frac{\partial^2\psi}{\partial z^2}=-r\zeta, \tag{13}$$

where ψ and ζ are dimensionless stream function and vorticity defined as

$$u=-\frac{1}{r}\frac{\partial \psi}{\partial z},\quad v=\frac{1}{r}\frac{\partial \psi}{\partial r}, \tag{14}$$

$$\zeta=\frac{\partial u}{\partial z}-\frac{\partial v}{\partial r}=-\frac{1}{r}\frac{\partial \psi^2}{\partial z^2}-\frac{\partial}{\partial r}\left(\frac{1}{r}\frac{\partial \psi}{\partial r}\right). \tag{15}$$

Initially, the entire system is assumed to be at uniform temperature, pressure and concentration which coincide with the bulk liquid condition

$$u=0,\quad v=-1,\quad \theta=0,\quad \varphi_i=0. \tag{16}$$

Boundary conditions are specified at three distinct locations: at the symmetric axes, at the far field and at the interface.

(1) *At the symmetric axis* ($z=0$):

$$\frac{\partial u}{\partial r}=0,\quad \frac{\partial v}{\partial r}=0,\quad \frac{\partial \theta}{\partial r}=0,\quad \frac{\partial \varphi_i}{\partial r}=0. \tag{17}$$

(2) *At the far field* ($r=\infty$):

$$u=0,\quad v=-1,\quad \theta=0,\quad \varphi_i=0. \tag{18}$$

(3) At the bubble surface, the vapor–liquid interface is treated as a free surface. Generally, free surface requires satisfaction of zero tangential stress at any point on the bubble surface. Let us assume the state of stress at one point on the free surface is described by the stress tensor **T**. Then the tangential stress can be expressed as [15]

$$(\mathbf{T}\bullet\mathbf{n})\bullet\mathbf{t}=(\mathbf{T}\bullet\mathbf{n})_{\mathbf{z}}\bullet\mathbf{t}_{\mathbf{z}}+(\mathbf{T}\bullet\mathbf{n})_{\mathbf{r}}\bullet\mathbf{t}_{\mathbf{r}} = \tau_{rz}n_r^2+\tau_{zz}n_rn_z-\tau_{rr}n_rn_z-\tau_{rz}n_z^2, \tag{19}$$

where n_r, n_z, t_r and t_z are unit vectors defined as

$$n_r=\frac{1}{\sqrt{1+(\partial h/\partial z)^2}},\quad n_z=\frac{-(\partial h/\partial z)}{\sqrt{1+(\partial h/\partial z)^2}},$$
$$t_r=\frac{\partial h/\partial z}{\sqrt{1+(\partial h/\partial z)^2}}=-n_z,\quad t_z=\frac{1}{\sqrt{1+(\partial h/\partial z)^2}}=n_r, \tag{20}$$

$h(z,t)$ denotes the bubble surface profile and $|\mathbf{n}|=|\mathbf{t}|=1$. Zero tangential stress means

$$\tau_{rz}n_r^2+\tau_{zz}n_rn_z-\tau_{rr}n_rn_z-\tau_{rz}n_z^2=0. \tag{21}$$

This condition determines the tangential velocity of the liquid on the bubble surface. Using Eqs. (4) and (5), we can rewrite Eq. (21) in the following forms:

$$\left(\frac{\partial v}{\partial r}+\frac{\partial u}{\partial z}\right)(1-h'^2)-2\left(\frac{\partial v}{\partial z}-\frac{\partial u}{\partial r}\right)h'=0, \tag{22}$$

where $h'=\partial h/\partial z$.

(4) Bubble surface temperature is assumed to be constant. This is consistent with the fact that the gas inside the bubble is assumed to be uniform in temperature and concentration due to internal circulation. Usually, the bubble surface temperature may vary with the location, but the degree of variation is very small. This can be explained as the result of strong diffusion in the vapor phase compared to diffusion in the liquid phase [2]. Internal circulation contributes to an evenly distributed temperature and concentration field inside the bubble and along the bubble interface [8]. The bulk liquid is subcooled and the degree of subcooling is the driving force of the bubble collapse. The degree of subcooling normally ranges from 3°C to 11°C depending on operating conditions. Compared to the degree of subcooling, the bubble surface temperature variation can be neglected.

(5) Finally, thermal equilibrium assumption at the interface leads to

$$\omega_{is}=f(T_s,p), \tag{23}$$

which means the mass fraction of species i can be determined from the interfacial temperature and pressure. ω_i represents the mass fraction of species i in the liquid and is defined as $\omega_i=\rho_i/\rho$. ρ_i is the mass concentration of species i, and ρ is the total mass concentration of the liquid. For the binary mixture,$\omega_i+\omega_j=1$. The properties of ammonia–water mixture were evaluated by McGahey's code [16] that uses source data from Reistad [17], Klein [18] and Ziegler [19].

Although the physical problem has been greatly simplified with many assumptions, it is still an unsteady, two-dimensional axisymmetric, moving boundary, phase change problem. These complexities make the mathematical problem as proposed not amenable to analytical solution. As a result, numerical method is

deemed to be a feasible approach. However, successful numerical solution demands more than a well-posed mathematical model. First, computational domain has to be well defined, which in our case requires consideration of irregular domain representation such as curvilinear coordinate system. Second, the moving boundary problem will add some complexity to the original governing equations.

3. Analysis

3.1. Bubble shape

In this study, a model proposed by Grace [20] is employed to simplify the prediction of the deformation of a fluid particle, otherwise the normal stress boundary condition must be used to determine bubble shape [21]. The approximate model is termed "double semi-ellipsoidal model" which assumes a distorted fluid particle is of a double semi-ellipsoidal shape as depicted in Fig. 1. The model has two equations to determine the two semi minor axes, b_1 and b_2, provided the semi major axis a is given. It assumes that the shape of a particle is primarily a function of hydrostatic pressure, surface tension, and external hydrodynamic pressure forces. The model considers the force balance the key factors dictating the bubble shape. The two equations proposed for double semi-ellipsoidal model are:

$$\frac{1}{4}Eo(1-e_1^2)^{1/2}(1-\cos\eta_1) = (1-e_1^2)^{1/2}\left[2-\frac{(2-e_1^2\sin^2\eta_1)}{(1-e_1^2\sin^2\eta_1)^{3/2}}\right]+\frac{We\sin^2\eta_1}{4k_3^2(1-e_1^2\sin^2\eta_1)}, \tag{24}$$

$$(8+Eo)\left(\frac{b_2}{a}\right)^3-4\left(\frac{b_2}{a}\right)^2-4=0, \tag{25}$$

where

$$e_1^2=\left(1-\frac{b_1^2}{a^2}\right),\quad k_3=\frac{1}{e_1^3}[\sin^{-1}e_1-e_1(1-e_1^2)^{1/2}]. \tag{26}$$

The above equation is numerically solved for e_1 and b_1. The model predicts a gradual and progressive flattening of the posterior portion of the bubble as we will see later. The surface tension tends to maintain a spherical shape whereas the dynamic forces act to flatten and hydrostatic forces act to elnogate. The final shape of the bubble is the balance of the three effects.

3.2. Bubble collapse rate

The bubble collapse rate is an important parameter in the analysis of bubble collapse dynamics and can be determined by the energy balance at the bubble interface

$$\dot{m}''\Delta h_{\mathrm{lv}}=-k_{\mathrm{l}}\left(\frac{\partial T}{\partial n}\right)_{\mathrm{s}}, \tag{27}$$

where $\dot{m}''$ is the total mass flux from vapor to liquid, which is actually the absorption rate in binary solutions. It is positive when the vapor mass is absorbed into the liquid. Δh_{lv} represents the heat released per unit mass of vapor absorbed and it is evaluated at constant pressure. $\Delta h_{\mathrm{lv}}=h_{\mathrm{v}}-h_{\mathrm{l}}-(x_{\mathrm{v}}-x_{\mathrm{l}})(\partial h/\partial x)_p$. The absorption rate can be evaluated by adding up the mass fluxes of component i and j, where mass flux of each component is the total effect of molecular diffusion and bulk convection [22]

$$\begin{aligned}\dot{m}'' &= \dot{m}_i''+\dot{m}_j''\\ &= \left[-\rho D_{ij}\left(\frac{\partial\omega_i}{\partial n}\right)_{\mathrm{s}}+\rho_i(v_{\mathrm{l,n}}-\dot{R})\right]\\ &\quad+\left[-\rho D_{ji}\left(\frac{\partial\omega_j}{\partial n}\right)_{\mathrm{s}}+\rho_j(v_{\mathrm{l,n}}-\dot{R})\right],\end{aligned} \tag{28}$$

where $v_{\mathrm{l,n}}$ is the normal velocity of the liquid at the interface. For a collapsing bubble, the liquid normal velocity at the bubble surface is related to the bubble surface moving velocity $\dot{R}$ through the mass balance across the interface [2]

$$\rho_{\mathrm{v}}(v_{\mathrm{v,n}}-\dot{R})=\rho_l(\mathrm{v}_{\mathrm{l,n}}-\dot{R}). \tag{29}$$

Neglecting the vapor velocity [12], we obtain

$$v_{\mathrm{l,n}}=\dot{R}(1-\rho_{\mathrm{v}}/\rho_{\mathrm{l}})\approx\dot{R}, \tag{30}$$

since $\rho_{\mathrm{v}}\ll\rho_{\mathrm{l}}$ is usually valid. This indicates the liquid normal velocity at the bubble interface is almost identical to the bubble interface moving velocity. If there is no mass transfer across the interface, $v_{\mathrm{l,n}}$ is strictly identical to $\dot{R}$. Making use of Eq. (30), we can simplify Eq. (28) into

$$\begin{aligned}\dot{m}'' &= \left[-\rho D_{ij}\left(\frac{\partial\omega_i}{\partial n}\right)_{\mathrm{s}}+\rho_i(v_{\mathrm{l,n}}-\dot{R})\right]\\ &\quad+\left[-\rho D_{ji}\left(\frac{\partial\omega_j}{\partial n}\right)_{\mathrm{s}}+\rho_j(v_{\mathrm{l,n}}-\dot{R})\right]=-\rho_v\dot{R},\end{aligned} \tag{31}$$

$\dot{R}=\mathrm{d}R/\mathrm{d}t$ is the rate of bubble radius reduction and is called bubble collapse rate in this study. It is so defined that it has a negative value when the bubble is shrinking. Now Eq. (27) can be rewritten in non-dimensional form

$$\dot{R}'=\frac{kT_\infty}{\rho_{\mathrm{v}}U_{\mathrm{t}}\Delta h_{\mathrm{lv}}D_0}\left(\frac{\partial\theta}{\partial n'}\right)_{\mathrm{s}}. \tag{32}$$

This equation shows that the temperature gradient around a bubble is one of the factors dictating the bubble collapse rate. Since the temperature gradient at the bubble surface is negative in our case, the bubble

collapse rate has a negative value, which is consistent with our sign convention.

3.3. Curvilinear coordinate system

A curvilinear coordinate system provides a flexible means to keep track of the changing boundary shape. The implementation of a curvilinear coordinate system is through mapping the physical domain (r,θ,z) to the computational domain (ξ,η,γ). To improve the resolution in certain regions of the physical field, the grid is made clustered toward the bubble interface so that the large variation in velocity, temperature and concentration can be captured truthfully. We know

$$\begin{aligned}\frac{\partial}{\partial r}&=\xi_r\frac{\partial}{\partial\xi}+\gamma_r\frac{\partial}{\partial\gamma},\\ \frac{\partial}{\partial z}&=\xi_z\frac{\partial}{\partial\xi}+\gamma_z\frac{\partial}{\partial\gamma}.\end{aligned}\tag{33}$$

The subscripts denote derivatives with respect to the corresponding variables. The question is to express ξ_r, ξ_z, γ_r, γ_z in terms of r_ξ, r_γ, z_ξ, z_γ. This is achieved by utilizing general 3-D mapping function [23]. Generally, we can configure a one-to-one mapping from (x,y,z) coordinate system to another coordinate system (ξ,η,γ): $(x,y,z)\Longleftrightarrow(\xi,\eta,\gamma)$. But in our case, the axisymmetric condition says,

$$x=r(\xi,\gamma)\cos\eta,\quad y=r(\xi,\gamma)\sin\eta,\quad z=z(\xi,\gamma).\tag{34}$$

Using the above equations and after some algebraic manipulation, we obtain [21]

$$\begin{aligned}\xi_x&=\frac{y_\eta z_\gamma-y_\gamma z_\eta}{J}=\frac{rz_\gamma}{J},\\ \xi_y&=\frac{x_\gamma z_\eta-x_\mu z_\gamma}{J}=0,\\ \xi_z&=\frac{x_\eta y_\gamma-x_\gamma y_\eta}{J}=-\frac{rr_\gamma}{J},\\ \eta_x&=\frac{y_\gamma z_\xi-y_\xi z_\gamma}{J}=0,\\ \eta_y&=\frac{z_\gamma x_\xi-z_\xi x_\gamma}{J}=\frac{1}{r},\\ \eta_z&=\frac{x_\gamma y_\xi-x_\xi y_\gamma}{J}=0,\\ \gamma_x&=\frac{y_\xi z_\eta-y_\eta z_\xi}{J}=-\frac{rz_\xi}{J},\\ \gamma_y&=\frac{z_\xi x_\eta-z_\eta x_\xi}{J}=0,\\ \gamma_z&=\frac{x_\xi y_\eta-x_\eta y_\xi}{J}=\frac{rr_\xi}{J},\end{aligned}\tag{35}$$

where J is the Jacobian given by

$$\begin{aligned}J&=\begin{vmatrix}x_\xi & y_\xi & z_\xi\\ x_\eta & y_\eta & z_\eta\\ x_\gamma & y_\gamma & z_\gamma\end{vmatrix}=\begin{vmatrix}r_\xi & 0 & z_\xi\\ 0 & r & 0\\ r_\gamma & 0 & z_\gamma\end{vmatrix}=r\begin{vmatrix}r_\xi & z_\xi\\ r_\gamma & z_\gamma\end{vmatrix}\\ &=rJ_2=r(r_\xi z_\gamma-r_\gamma z_\xi)\end{aligned}\tag{36}$$

and $r_\xi,r_\gamma,z_\xi,z_\gamma$, etc. are called the metrics of the transformation. Substituting all the available derivatives back into Eq. (33), we have

$$\begin{aligned}\frac{\partial}{\partial r}&=\xi_r\frac{\partial}{\partial\xi}+\gamma_r\frac{\partial}{\partial\gamma}=\frac{r}{J}\left(z_\gamma\frac{\partial}{\partial\xi}-z_\xi\frac{\partial}{\partial\gamma}\right),\\ \frac{\partial}{\partial z}&=\xi_z\frac{\partial}{\partial\xi}+\gamma_z\frac{\partial}{\partial\gamma}=\frac{r}{J}\left(-r_\gamma\frac{\partial}{\partial\xi}+r_\xi\frac{\partial}{\partial\gamma}\right).\end{aligned}\tag{37}$$

These equations will be used to transform governing equations and associated boundary conditions from axisymmetric system into the curvilinear system. Besides above equations, Laplace operator is frequently used in Navier–Stokes equation, and it can be expressed in the curvilinear coordinates as

$$\begin{aligned}\nabla^2_{\xi\eta}=\frac{1}{J}\Bigg[&\frac{\partial}{\partial\xi}\left(rA\frac{\partial}{\partial\xi}\right)+\frac{\partial}{\partial\xi}\left(rB\frac{\partial}{\partial\gamma}\right)\\ &+\frac{\partial}{\partial\gamma}\left(rB\frac{\partial}{\partial\xi}\right)+\frac{\partial}{\partial\gamma}\left(rC\frac{\partial}{\partial\gamma}\right)\Bigg],\end{aligned}\tag{38}$$

where

$$A=\frac{z_\gamma^2+r_\gamma^2}{J_2},\quad B=-\frac{z_\xi z_\gamma+r_\xi r_\gamma}{J_2},\quad C=\frac{z_\xi^2+r_\xi^2}{J_2}.\tag{39}$$

With the above knowledge, we are able to rewrite the governing equation and associated boundary conditions in terms of the curvilinear boundary-fitted coordinates. But before doing that, let us consider the moving boundary feature since it has to be incorporated as an integral part of our governing equation in the curvilinear coordinate system.

3.4. Moving boundary feature

For a moving boundary problem, the boundary changes its spatial location with time. In our case, the bubble surface is moving as the bubble collapses. There exist several techniques for tracking arbitrarily shaped interfaces, each has its pros and cons. A clear-cut boundary between vapor and liquid is preferable in order to investigate the interface behavior and to evaluate key quantities such as temperature gradient near the bubble surface. Lagrangian methods maintains the interface as a discontinuity and explicitly tracks its evolution, therefore the boundary conditions can be applied at the exact location of the interface. To apply Lagrangian methods, a boundary-fitted grid is created such that the grid dynamically conforms to the moving interface. That is, the grid itself is also moving. Mathematically speaking, it is expressed as

$$\xi=\xi(r,z,t),\quad \gamma=\gamma(r,z,t),\tag{40}$$

where the (r,z) domain changes with time while (ξ,γ) domain is fixed. The time derivative of a physical quantity, say vorticity $\xi(r,z,t)$, on the moving domain

(r,z) can be related to its counterpart in the fixed (ξ,γ) domain as

$$\left(\frac{\partial\zeta}{\partial t}\right)_{rz} = \left(\frac{\partial\zeta}{\partial t}\right)_{\xi\gamma} - \frac{r}{J}\left[(\dot{r}z_\gamma - \dot{z}r_\gamma)\zeta_\xi + (-\dot{r}z_\xi + \dot{z}r_\xi)\zeta_\gamma\right]. \tag{41}$$

The $\dot{r}$ and $\dot{z}$ are the velocity components of the image of (ξ,γ) moving on the (r,z) domain and can be approximated by the first-order backward difference. Making use of Eqs. (37), (38) and (41), we are able to rewrite Eqs. (12) and (13) in terms of the moving curvilinear coordinates [21]

$$J\frac{\partial\zeta}{\partial t} + \frac{\partial(U^*\zeta)}{\partial\xi} + \frac{\partial(V^*\zeta)}{\partial\gamma} - \frac{J(u-\dot{r})\zeta}{r} = \frac{1}{Re}\left[(rA\zeta_\xi)_\xi + (rB\zeta_\gamma)_\xi + (rB\zeta_\xi)_\gamma + (rC\zeta_\gamma)_\gamma - \frac{J\zeta}{r^2}\right], \tag{42}$$

$$(rA\psi_\xi)_\xi + (rB\psi_\gamma)_\xi + (rB\psi_\xi)_\gamma + (rC\psi_\gamma)_\gamma - 2(z_\gamma\psi_\xi - z_\xi\psi_\gamma) = -r\zeta J, \tag{43}$$

where U^* and V^* are contravariant velocities for the moving boundary problem expressed as

$$U^* = r[z_\gamma(u-\dot{r}) - r_\gamma(v-\dot{z})], \tag{44}$$

$$V^* = r[-z_\xi(u-\dot{r}) + r_\xi(v-\dot{z})]. \tag{45}$$

These velocity terms naturally arise during the mathematical transformation. Following the same procedure, we can derive the energy and species conservation equation in the curvilinear system

$$J\frac{\partial\theta}{\partial t} + U^*\frac{\partial\theta}{\partial\xi} + V^*\frac{\partial\theta}{\partial\gamma} = \frac{1}{RePr}\left[(rA\theta_\xi)_\xi + (rB\theta_\gamma)_\xi + (rB\theta_\xi)_\gamma + (rC\theta_\gamma)_\gamma\right], \tag{46}$$

$$J\frac{\partial\varphi_i}{\partial t} + U^*\frac{\partial\varphi_i}{\partial\xi} + V^*\frac{\partial\varphi_i}{\partial\gamma} = \frac{1}{ReSc}\left[(rA\varphi_{i_\xi})_\xi + (rB\varphi_{i_\gamma})_\xi + (rB\varphi_{i_\xi})_\gamma + (rC\varphi_{i_\gamma})_\gamma\right]. \tag{47}$$

3.5. Grid generation

The physical domain must be covered by a mesh so that conservation laws can be applied onto each discrete element. In the present study, elliptical scheme [24] is used to perform the grid generation. Fig. 2 shows a 70×70 boundary-fitted grid around a rising bubble, wherein the grid is clustered toward the bubble surface. The grid must be regenerated at each time step so that it can dynamically adapt to the changing shape of a collapsing bubble.

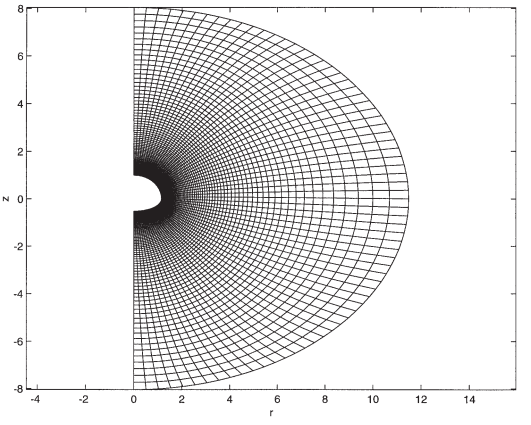

Fig. 2. Boundary-fitted grid around a collapsing bubble.

3.6. Algorithm

The problem, from the numerical point of view, is to solve Eqs. (42), (43), (46) and (47) subject to all of the initial and boundary conditions specified above. Since the momentum equations are not coupled with the energy and species continuity equations, we can solve them separately. The energy equation, however, is coupled with the species continuity equation and they have to be solved simultaneously. To start the computation, the grid velocity for the very first time step must be guessed [2] or determined from a similar theoretical solution [1]. Thereafter, they are computed numerically from the previous time step. It turned out that this approach produced no adverse effect on the bubble collapse rate for a pure substance [1]. The iterative solution algorithm is outlined in Fig. 3. The algorithm requires regenerating the adaptive grid and performing metrics calculation at each time step.

4. Results and discussion

To assess the accuracy of the numerical method developed in this study, the flow field surrounding a solid sphere is numerically solved. The result is compared to the flow visualization experiment results, see [21] for details. This exercise is a validation of the flow solver developed in our program. It justified the curvilinear system transformation involved in our algorithm, proved the efficiency and stability of discretization procedure employed in this study, and finally confirmed that the number of nodes used (70×70) is sufficient to provide adequate accuracy and the finite difference solution is independent of the grid size. Fig. 4 demonstrates good agreement between the experimental flow visualization and streamlines obtained from our numerical simulation.

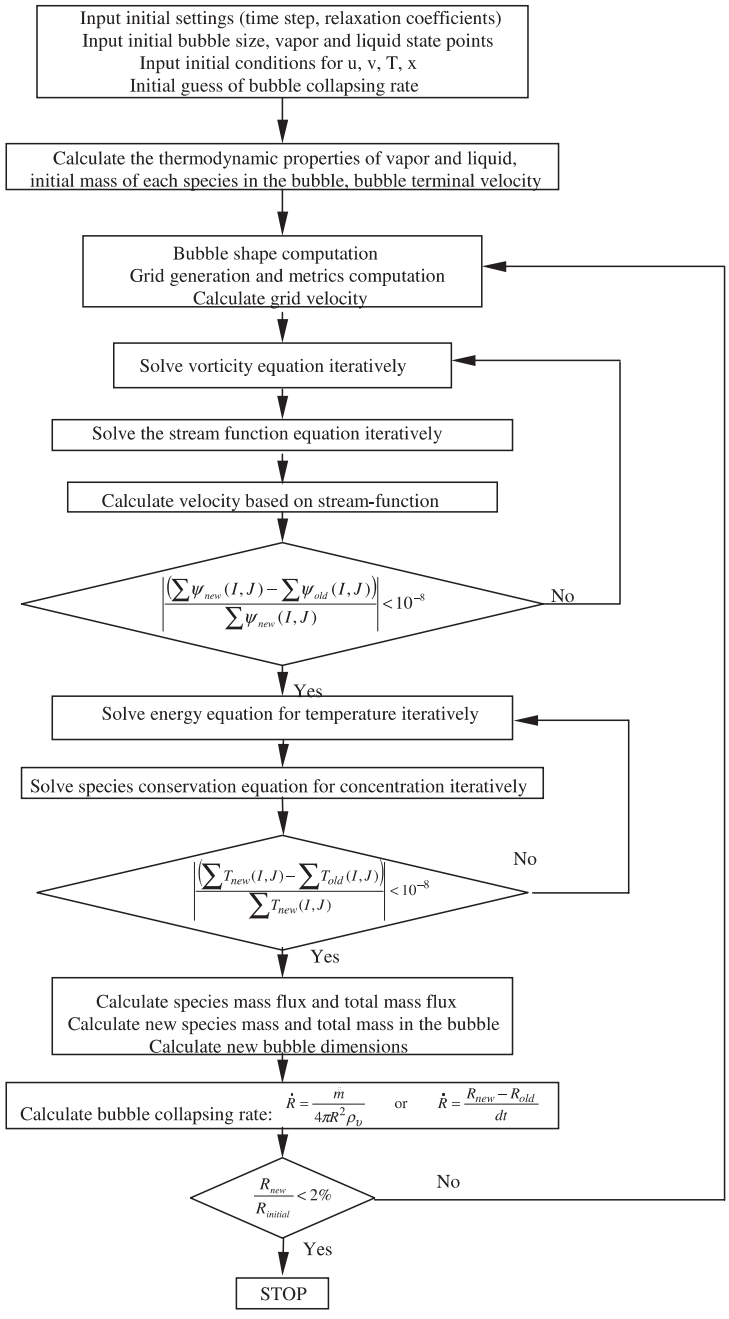

Fig. 3. Overall solution algorithm flowchart.

We now proceed to analyze the bubble collapse problem. Table 1 lists typical operating conditions of an ammonia-water generator–absorber-heat-eXchange (GAX) absorber. The initial volume equivalent bubble diameter is 4 mm. Fig. 5 shows a sequence of instantaneous flow, temperature and species concentration patterns. Initially, the bubble takes an oblate ellipsoidal shape with a longer anterior semi axis than the posterior semi axis. The impact of higher temperature and ammonia concentration at the bubble surface is limited to the area close to the bubble interface while most of the liquid is undisturbed. As time proceeds, the bubble is being absorbed, the heat released at the bubble interface is dissipated into the bulk liquid through convection and, the liquid around the bubble is being heated. The bubble volume and the vapor mass encapsulated within

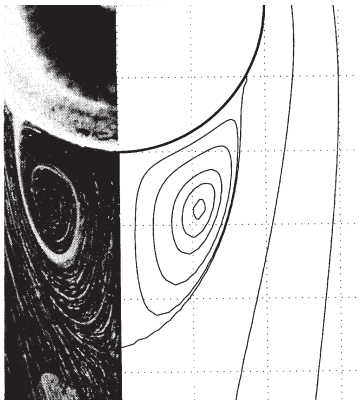

Fig. 4. Comparison of stream function contours with experimental visualization. (1) Left: Taneda's [25] flow visualization $Re = 73.6$. (2) Right: current numerical simulation $Re = 73.6$.

Table 1
Typical absorber operating conditions

Vapor concentration of ammonia	0.996
Bulk liquid concentration of ammonia	0.1
Bulk liquid temperature (°C)	94.7
Pressure (kPa)	501

are gradually diminishing. As the bubble shrinks, its shape changes from double semi-ellipsoidal shape progressively toward spheroid. At $t = 3.0$ s, the bubble is about 35% of the initial size and has become fairly close to be spherical.

Although a circulating flow pattern in the form of wakes is considered as an inherent characteristic for the flow around a blunt object, Fig. 5 shows no wake behind the collapsing bubble. The existence of a standing wake in the flow past a solid body is believed to be a consequence of boundary-layer separation. The no-slip condition at the body surface causes a deficit of momentum in the fluid nearest the boundary compared to what it would have in the free stream or potential flow. Thus, the fluid in this boundary region does not retain enough kinetic energy to overcome the pressure rise at the rear of the body, and breaks away into the main body of fluid. However, such argument cannot be used in separation at a zero-shear-stress interface because the fluid does not come to rest at the interface. Therefore, the loss of kinetic energy of the fluid in the boundary layer is not as significant as that in the no-slip case. Batchelor [26] argued that for a free surface the boundary layer separation is a consequence of the development of standing wakes behind the body due to the accumulation of vorticity brought to this area by convection, rather than vice versa. This evolution-type view is supported by the fact that while separation in laminar flow is always accompanied by standing wakes, the standing wakes behind a body may exist without separation [27,28]. In line with the viewpoint expressed above, the crucial condition for existence of standing wakes (or boundary layer separation) is the generation of vorticity at a sufficient rate. The vorticity generation depends on bubble curvature and boundary condition at the bubble surface. First, larger curvature due to bubble deformation leads to greater vorticity generation while smaller curvature results in less vorticity generation [9,21]. As *We* increases, bubble deformation increases, so does the maximum surface curvature and vorticity. Second, the zero-shear-stress inhibits the vorticity generation as opposed to the no-slip condition. For a fixed size bubble with enough curvature or deformation, a standing wake does exist but is weaker than that behind a rigid object with the same geometry [9,21]. Since the bubble is collapsing and approaching spherical shape, the vorticity generation becomes weaker while bubble curvature becomes smaller as the collapse proceeds. In addition, bubble life span is fairly short, there is not enough time for vorticity to be accumulated and convected downstream to build a standing wake. Therefore, the decreasing curvature and short life span of the bubble are two major factors that prevent wake formation behind a collapsing bubble. Given the fact that no wake is formed behind a collapsing bubble, it appears that potential flow could be a valid solution to the entire external flow field around a bubble. However, the velocity derivatives given by the potential flow solution would not satisfy zero tangential stress condition at the bubble surface [8,21]. Moreover, fore-and-aft symmetry does not hold anymore, no potential flow solution exists for a non-spherical bubble undergoing progressive shape change. The wake would have accelerated the bubble absorption if it were created. The absence of wake implies that the flow field is less agitated. The impact of temperature and concentration variation is limited to the area adjacent to the bubble surface and the traveling path of the bubble. From absorber design point of view, it indicates greater absorber size.

Bubble collapse is a transient process involving simultaneous volume reduction and shape alteration. Fig. 6 illustrates the history of a collapsing bubble. The subcooling of the ambient liquid is about 5.56°C, which corresponds to $Ja = 6.28$. The bubble is traveling at its terminal velocity that is approximately 0.206 m/s given by Grace's correlation. Fig. 6 demonstrates the instantaneous bubble size, bubble shape and associated elapse time and the exact location of the bubble relative to its initial location. It shows that the bubble shape progressively evolves into spherical shape as it shrinks in size, primarily because the bubble base becomes more spherical. About 0.9 s after its introduction to the subcooled ambient liquid, the bubble equivalent diameter is less than 2% of its initial diameter which is considered as the end of the bubble life in the present study. Bubble life span and its traveling distance depend largely on the

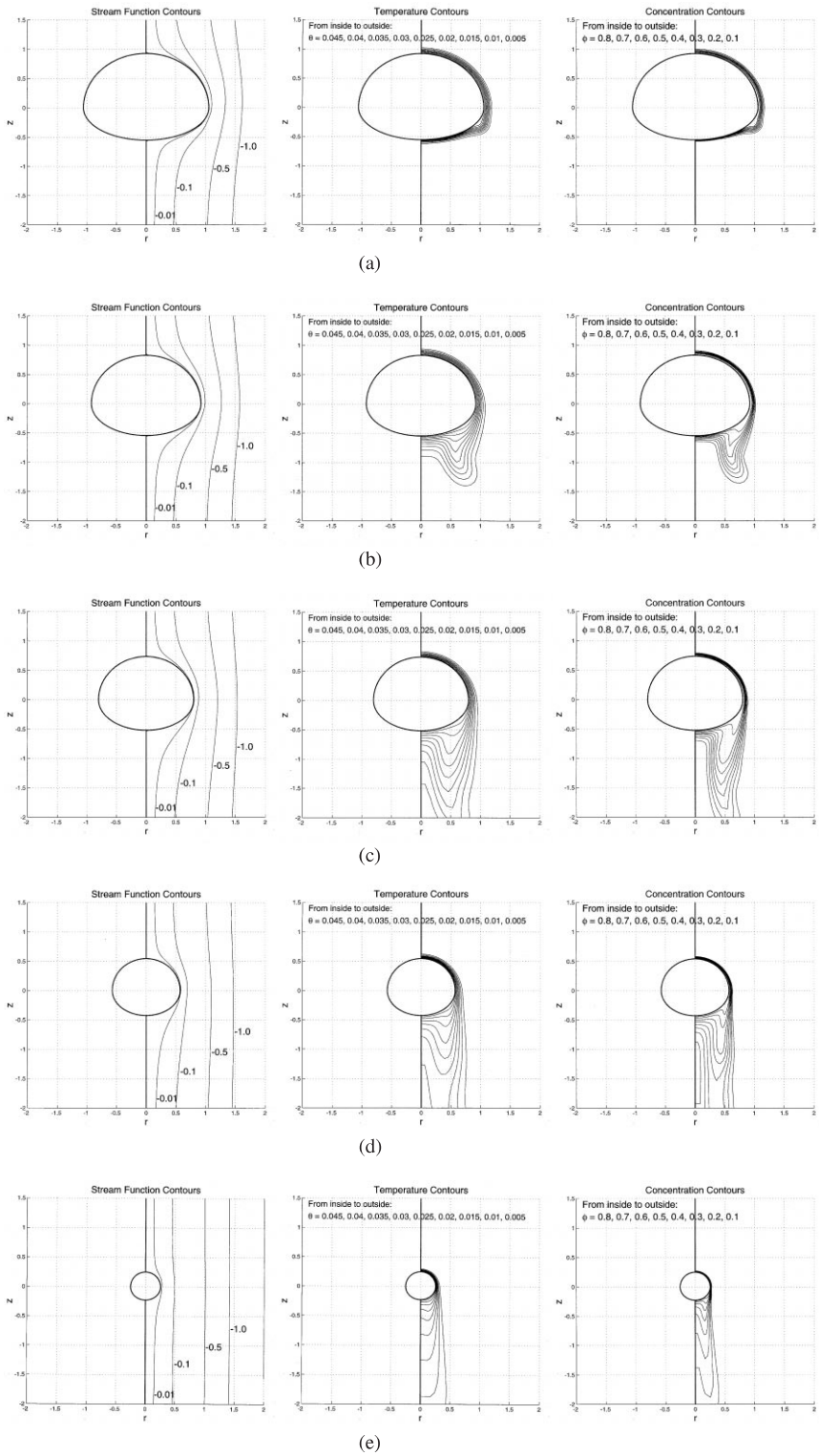

Fig. 5. Dimensionless streamlines, temperature and species concentration contours ($Re = 100$, $We = 3.4$, $D_0 = 4$ mm): (a) $t = 0.1$ s; (b) $t = 0.5$ s; (c) $t = 1.0$ s; (d) $t = 2.0$ s; (e) $t = 3.5$ s.

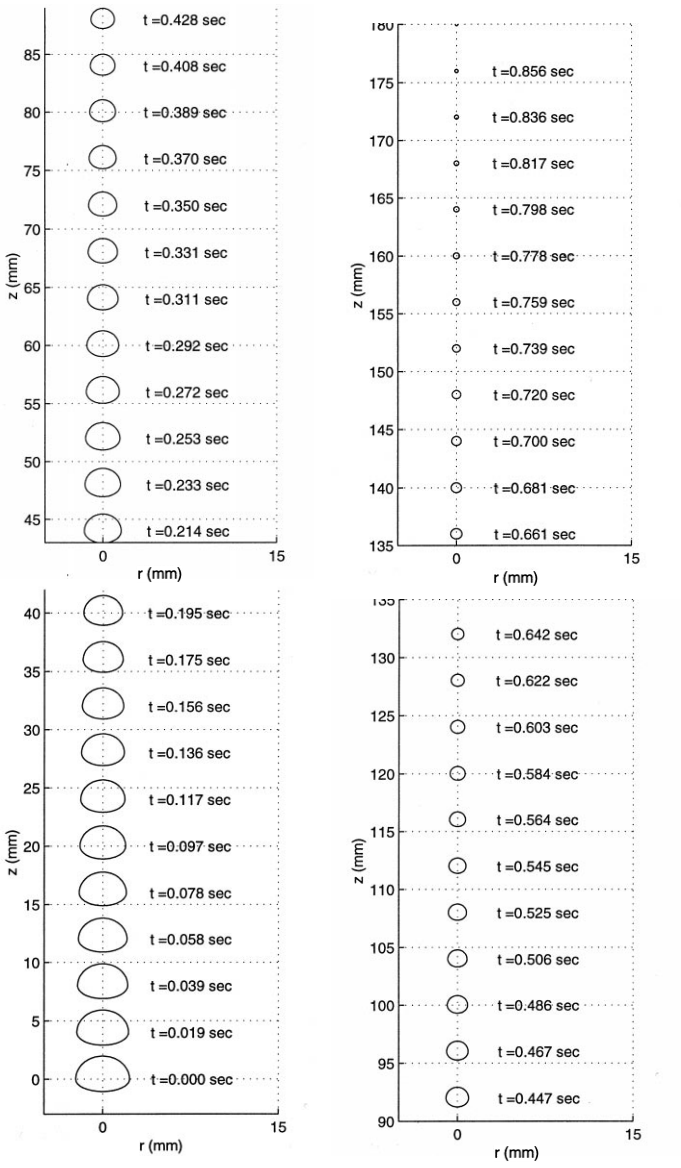

Fig. 6. Bubble collapse process ($We = 3.4$, $Re = 2290$, $Ja = 6.28$, $D_0 = 4$ mm).

initial bubble size. For the case considered in Fig. 6, the distance that the bubble travels in the translatory motion during its lifetime is around 180 mm, which can be viewed as a first-order approximation of the absorber size.

Bubble collapse time increases with the bubble size because more vapor is enclosed in the bubble. However, the quantitative relationship between the collapse time and the bubble size is not so intuitive. Fig. 7 presents some basic understanding. Bubbles with different sizes may have different shapes and terminal velocities, which could significantly change the flow pattern and temperature, concentration distribution around the bubbles. Table 2 associated with Fig. 8(a) illustrates the bubble collapse time as a function of initial bubble diameter and Reynolds number. The shaded cells in Table 2 indicate that Reynolds numbers are corresponding to the actual terminal velocities based on the bubble diameters. As the bubble diameter increases, *Re* also increases. The eventual effect is that the bubble collapse time is longer for larger bubbles but is less extended than it would have been if it were at smaller Reynolds number. Fig. 8(b) presents the bubble traveling distances at different initial bubble diameters and Reynolds number. The distance can be viewed as an indication of the desired bubble column height. For instance, a bubble with 6 mm initial

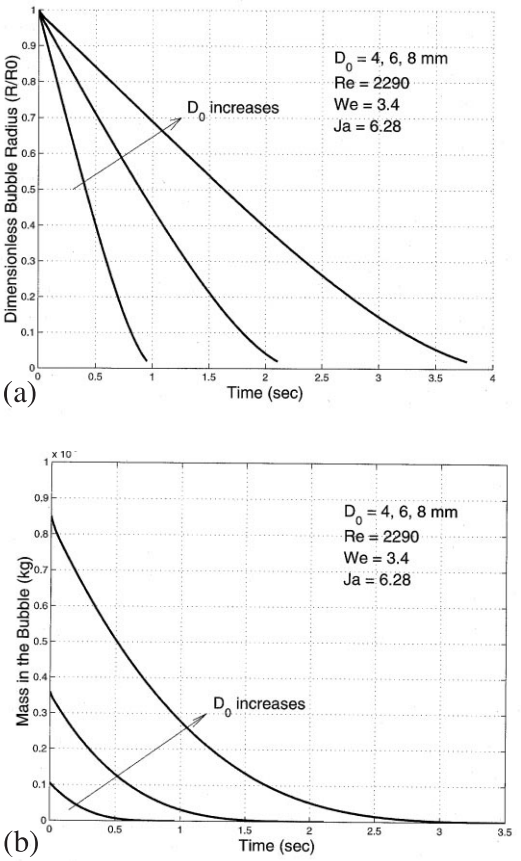

Fig. 7. Influence of initial bubble size on the collapse behavior: (a) radius; (b) mass.

Table 2
Bubble collapse time for different bubble diameters and Reynolds number

	$Re = 2290$	$Re = 3298$	$Re = 4266$
D_0 = 4 mm	0.953	0.808	0.727
D_0 = 6 mm	2.109	1.796	1.628
D_0 = 8 mm	3.773	3.218	2.908

diameter moving at its terminal velocity (corresponding to $Re = 3298$) in a subcooled liquid with $Ja = 6.28$ and ambient concentration $X_\infty = 0.1$ will have traveling distance of 354.6 mm.

5. Conclusion

A comprehensive model has been developed which reasonably describes the bubble collapse dynamics in a subcooled binary mixture. The results are subject to further experimental verification. Assessing the accuracy of the numerical model proved to be difficult because of

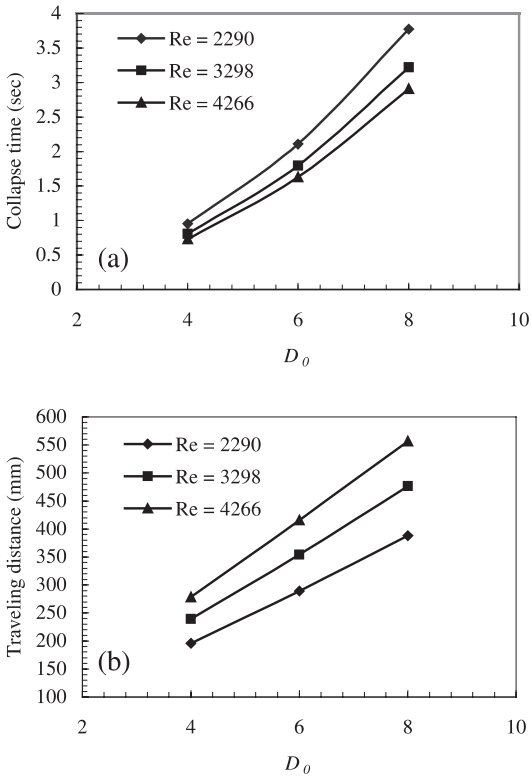

Fig. 8. Bubble collapse time and traveling distance as a function of initial bubble diameter and Reynolds number ($We = 3.4$, $Ja = 6.28$): (a) collapse time; (b) traveling distance.

limited research on non-spherical bubble collapse in the binary solution. However, this study has provided insights into fundamental bubble absorption dynamics in binary solutions taking placing in GAX absorber.

1. Numerical results demonstrate that the bubble progressively approaches spherical shape as it collapses.
2. Rapid reduction of bubble size and zero tangential stress at the bubble interface suppress the vorticity generation and accumulation, which prevents boundary layer separation and wake development.

References

[1] D.D. Wittke, B.T. Chao, Collapse of vapor bubble with translatory motion, J. Heat Transfer 89 (1967) 17–24.
[2] T.L. Merrill, H. Perez-Blanco, Combined heat and mass transfer during bubble absorption in binary solutions, Int. J. Heat Mass Transfer 40 (3) (1997) 589–603.
[3] J.S. Hadamard, Mouvement permanent lent d'une sphere liquide et visquesuse dans une liquide visqueux, C. R. Acad. Sci. 152 (1911) 1735–1738.
[4] W. Rybczynski, On the translatory motion of a fluid sphere in a viscous medium, Bull. Int. Acad. Pol. Sci. Lett. Cl. Sci. Math. Nat., Series A (1911) 40–46.

[5] V.G. Levich, Motion of gaseous bubbles with high Reynolds number, Zhn. Eksp. Teor. Fiz. 19 (1949) 18–24.
[6] A.E. Hamielec, T.W. Hoffman, L.L. Ross, Viscous flow around spheres with and without radial mass flux, AIChE 13 (2) (1967) 212–219.
[7] D.C. Brabston, H.B. Keller, Viscous flows past spherical gas bubbles, J. Fluid Mech. 69 (1975) 179–189.
[8] R. Clift, J.R. Grace, M.E. Weber, Bubbles Drops and Particles, Academic Press, New York, 1978, pp. 27–176.
[9] G. Ryskin, L.G. Leal, Numerical solution of free-boundary problems in fluid mechanics. Part 1. The finite difference technique, J. Fluid Mech. 148 (1984) 1–17.
[10] G. Ryskin, L.G. Leal, Numerical solution of free-boundary problems in fluid mechanics. Part 2. Buoyancy-driven motion of a gas bubble through a quiescent liquid, J. Fluid Mech. 148 (1984) 19–35.
[11] S. Takagi, Y. Matsumoto, Numerical analysis of a single rising bubble using boundary fitted coordinate system, JSME, Series B 10 (1) (1997) 42–50.
[12] L.W. Florschuetz, B.T. Chao, On the mechanics of vapor bubble collapse, J. Heat Transfer 87 (1965) 209–220.
[13] M.S. Plesset, S.A. Zwick, A nonsteady heat diffusion problem with spherical symmetry, J. Appl. Phys. 23 (1952) 95–98.
[14] Y.M. Chen, F. Mayinger, Measurement of heat transfer at the phase interface of condensing bubbles, Int. J. Multiphase Flow 18 (6) (1992) 877–890.
[15] S. Middleman, Modeling Axisymmetric Flows, Dynamics of Films, Jets and Drops, Academic Press, New York, 1995, pp. 1–7.
[16] K. McGahey, The modeling and optimization of a generator–aborber heat exchange, absorption heat pump using modular steady state simulation, Master thesis, The Ohio State University, 1993.
[17] B. Reistad, Thermodynamic properties of ammonia–water mixtures, Technical report to Electrolux, Sweden, report 11108, 1969.
[18] S.A. Klein, Thermodynamic properties of ammonia–water mixtures, ASME transactions, Adv. Energy Sys. (1993).
[19] B. Ziegler, C. Trepp, Equation of state for ammonia–water mixtures, Int. J. Refrigeration 7 (2) (1984).
[20] J.R. Grace, T. Wairegi, Shapes of Fluid Particles, Transport Processes in Bubbles, Drops, and Particles, Hemisphere, Washington, DC, 1992, pp. 133–145.
[21] J. Cao, Mechanics of bubble collapse in binary mixture with simultaneous heat and mass transfer, Ph.D. dissertation, Ohio State University, 1999.
[22] R.B. Bird, W.E. Stewart, E.N. Lightfoot, Transport Phenomena, Wiley, New York, 1960, pp. 496–503.
[23] W. Shyy, Computational Modeling for Fluid Flow and Interfacial Transport, Part II, Elsevier, New York, 1994.
[24] J.F. Thompson, Z.U.A. Wasri, C.W. Mastin, Boundary-fitted coordinate system for numerical solution of partial differential equations – a review, J. Comput. Phys. 47 (1) (1982).
[25] S. Taneda, J. Phys. Soc. Jpn. 11 (1956) 1104–1108.
[26] G.K. Batchelor, An Introduction to Fluid Dynamics, Cambridge University Press, New York, 1967 (Chapter 4-5).
[27] L.G. Leal, A. Acrivos, The effect of base bleed on the steady separation flow past bluff objects, J. Fluid Mech. 39 (1969) 735–752.
[28] V.Y. Rivkind, G. Ryskin, Flow structure in motion of a spherical drop in a fluid medium at intermediate Reynolds numbers, Fluid Dyn. 11 (1976) 5–12.